Chinmo is a novel regulator of differential Hippo signaling response within a single developing organ

Shreeharsha Tarikere[1,2] *, Tarun Kumar[1,3] *, Guillem Ylla[1,4], Cassandra G. Extavour[1,3,5]

Department of Organismic & Evolutionary Biology, Harvard University, Cambridge MA, USA.

1. Current address: Department of Human Genetics, McGill University, Montréal, Québec, Canada
2. Howard Hughes Medical Institute, Bethesda MD, USA
3. Current address: Laboratory of Bioinformatics and Genome Biology, Faculty of Biochemistry, Biophysics and Biotechnology, Jagiellonian University, Kraków, Poland
4. Department of Molecular & Cellular Biology, Harvard University, Cambridge MA, USA

* Contributed equally

Correspondence: guillem.ylla@uj.edu.pl, extavour@oeb.harvard.edu

ABSTRACT

Orchestrated control of proliferation of multiple cell types is essential for building a healthy organ. Here we use larval ovary development in *Drosophila melanogaster* as a model to understand the homeostasis of somatic and germ line cells in the formation of the female adult reproductive organ. We previously showed that the highly conserved Hippo signaling pathway regulates proliferation of both germ line and somatic cells in the *D. melanogaster* larval ovary. Response to Hippo signaling appeared to be mediated by different genetic mechanisms in germ line and soma, but the mechanism allowing distinct responses to the same signaling pathway remained unknown. Here we perform cell type-specific RNA-Seq of isolated germ line and somatic cells from the developing ovary at multiple time points spanning the formation of germ line stem cell niches, in either a Hippo signaling loss- or gain-of-function genetic background. Applying network analysis to these data revealed a novel regulator of ovarian development, the transcription factor *chinmo*. Subsequent experimental validation showed that *chinmo* acts as a key germ cell-specific translator of Hippo signaling in the developing ovary, allowing the Hippo signal to be transduced in cell type-specific ways in germ line and somatic cells within the same organ.

KEY WORDS: Yorkie, ovariole number, FACS, RNA-Seq, Larva, Ovary, *Drosophila,*

INTRODUCTION

Animal organs are not heterogeneous masses of cells. Instead, they are composed of multiple cell types that contribute to the same organ, but have distinct gene expression profiles, morphologies, behaviours, and functions. In most organ systems, all these distinct cell types are somatic cells derived from the same germ layer (Barresi and Gilbert 2023). An important exception to this rule is found in the gonads (ovaries and testes), which contain both somatic cells of mesodermal origin, and cells of the germ line, destined to make eggs and sperm (Extavour 2007). Gonads are typically assembled after the specification of germ layers and of the germ line, but before gametogenesis begins. During gonadogenesis, somatic and germ cells proliferate, exchange neighbors, change their shapes and gene expression profiles, and create the final functional anatomical organization of the gonad. As for other systems of organogenesis, cell-cell signaling is crucial for this process. However, each unique cell type within the developing organ often has a distinct, cell type-appropriate response to the same incoming signals, allowing correct organ formation and function. Here we use the *Drosophila melanogaster* (fruit fly) ovary as a study system to elucidate how different cell types within the same organ can differently transduce the same signaling inputs during development.

A single adult ovary in *D. melanogaster* is made up of an estimated 26 distinct cell types (Rust et al. 2020) that are assembled into 16-23 tubular egg producing subunits called ovarioles (Büning 1994), making it an excellent model to study the regulation of organ size and subunit number (Sarikaya and Extavour 2015; Kumar et al. 2020). Ovariole number varies by up to four orders of magnitude across insect species, and in some insects, including Drosophilids, it is positively correlated with egg-laying and therefore fitness (Church et al. 2021; David 1970). In *Drosophila* species, ovariole number is established in the larval stages and determined by the number of stacks (called terminal filaments: TFs) of a specific type of somatic cell (terminal filament cells: TFCs) (King 1968,Honěk 1993,Markow 2007,Hodin 2009,Green 2012,Sarikaya

59 2019). The number of these stacks of cells, in turn, is determined by the number and stacking
60 dynamics of the component TFCs. We previously showed that TFC proliferation, and therefore
61 ovariole number, is regulated by the Hippo (Hpo) signaling pathway, which affects both TFC and
62 germ cell numbers (Sarikaya and Extavour 2015).

63 First discovered as a network of tumor overgrowth factors in *D. melanogaster* (Tapon et
64 al. 2002; Dong et al. 2007; Xu et al. 1995; Wu et al. 2003), the Hpo signaling pathway regulates
65 organ size, growth, cell proliferation and cell fate determination in animals. In the developing fruit
66 fly ovary, this pathway can regulate proliferation both cell-autonomously (based on cell-intrinsic
67 Hpo signaling activity) and non-cell autonomously (activity in one cell can affect proliferation in a
68 different cell) (Sarikaya and Extavour 2015). Regulation of cell proliferation in both the soma and
69 the germ line is essential for the normal development of the ovary, including species-specific
70 ovariole number. Members of the Hippo signaling pathway are expressed ubiquitously across
71 multiple distinct ovarian cell types that nevertheless have different proliferation dynamics
72 (Sarikaya and Extavour 2015). This begs the question of how differential regulation of Hpo
73 signaling may be achieved despite the potential for ubiquitous activation.

74 The canonical Hippo signaling pathway functions through regulating shuttling of the
75 transcriptional activator Yorkie (Yki) in and out of the nucleus. This shuttling is regulated by the
76 function of the serine-threonine kinase Hpo in conjunction with a cascade of kinases that ends
77 with the phosphorylation of Yki, preventing its nuclear localisation (Oh and Irvine 2008; Huang et
78 al. 2005). Under this model, unphosphorylated Yki enters the nucleus to form tissue-specific
79 transcriptional regulatory complexes (Slattery et al. 2013) with loading proteins like Scalloped (Sd)
80 and Homothorax (Hth). These transcription cofactor complexes bind to DNA and activate a wide
81 range of target genes, including many necessary for growth and proliferation (Wu et al. 2008;
82 Zhang et al. 2008; Zhao et al. 2008). Phosphorylation of Yki by other kinases, including Nemo-
83 like kinase and AMP-activated protein kinase, can either prevent or enhance Yki's targeting by

84 the canonical Hpo kinases, allowing a Hpo-independent mode of Yki regulation (Moon et al. 2017;
85 Wang et al. 2015). Furthermore, changes in the binding dynamics of Sd, the coactivator of Yki,
86 adds another layer of Yki regulation (Manning et al. 2024). Lastly, mechanical stress and proximity
87 of cell membranes during cell growth and proliferation can also regulate the Hpo signaling activity
88 (Zhao et al. 2007). Across animals, the Hpo pathway regulates multiple cellular processes *via* Yki
89 target genes, including cell size, cell proliferation, adhesion and apoptosis (Zheng and Pan 2019),
90 while interacting with other signaling pathways such as JAK-STAT, Notch, Hedgehog and EGFR
91 (Besse 2005,Matsuoka 2013,Sarikaya 2015,Yatsenko 2021,Song 2007,Kumar 2020) .

92 Previously, we showed that Hpo pathway activity regulates cell proliferation in multiple *D.*
93 *melanogaster* ovarian cell types, which in turn can determine the numbers of TFCs, TFs and
94 ultimately ovarioles (Sarikaya and Extavour 2015). RNAi-mediated knockdown of *hpo* or *wts* in
95 somatic cells increased TF and TFC number, while RNAi against *yki* decreased the numbers of
96 both cell types (Sarikaya and Extavour 2015). In this context, we demonstrated that the Hpo
97 pathway interacts with the EGFR pathway to regulate numbers of another somatic cell type, called
98 intermingled cells (Sarikaya and Extavour 2015) and with JAK-STAT signaling to regulate TFC
99 proliferation and the homeostasis between intermingled cells and germ cells (Sarikaya and
100 Extavour 2015). Furthermore, our RNAi screen in a *hpo* knockdown background in the larval ovary
101 identified a gene interaction network implicating all known conserved animal signaling pathways
102 in regulating *D. melanogaster* ovary development and function, including establishment of correct
103 ovariole number (Kumar et al. 2020).

104 To our surprise, our previous study showed that in contrast to somatic cells, *hpo*
105 knockdown did not affect germ cell number (Sarikaya and Extavour 2015). However, *yki*
106 knockdown reduced germ cell number significantly, as it did in somatic cells. This result suggested
107 the existence of a Hpo-independent mechanism of Yki activity in the germ cells (Sarikaya and
108 Extavour 2015). However, a mechanistic explanation for the differential response of germ cells

109 and somatic cells to these Hpo signaling components remains lacking. Given the variation in
110 outcomes of Hpo pathway abrogation in the germ cells and the somatic cells, we sought to use
111 cell type-specific transcriptional profiling to identify distinct gene regulatory responses to *hpo* or
112 *yki* activity in soma versus germ line. Here we present the results of this approach, wherein we
113 analyze stage- and tissue-specific transcriptomic datasets generated in three distinct genetic
114 backgrounds to assess the role of Hpo signaling and its interacting pathways in the cell types of
115 the developing *D. melanogaster* larval ovary. We reveal the transcription factor Chinmo as a
116 putative novel regulator of germ cell-specific Hpo-dependent activity and provide experimental
117 validation of this regulatory interaction in the developing ovary. Further, we provide evidence that
118 *chinmo* regulates the previously observed (Sarikaya and Extavour 2015) non-autonomous effect
119 that Hpo activity in germ cells exerts on neighboring somatic cells. Thus, our results show how
120 variation in the expression of cell type-specific targets can produce distinct proliferation response
121 outcomes to the same signaling inputs within a developing tissue.

122

123 **RESULTS**

124

125 ***hpo* and *yki* knockdown in somatic and germ line tissues**

126 *D. melanogaster* ovaries are made up of subunits called ovarioles (Figure 1A), whose number is
127 established at the third larval instar stage, 72-120 hours after egg laying (hAEL) at 25ºC (Figure
128 1B) (King 1970). The number of ovarioles in the adult directly corresponds to the number of TFs
129 formed in the larval ovary (Figure 1B), because TFs are neither formed nor destroyed during the
130 pupal phase that separates larva from adult (King 1970). The Hpo signaling pathway regulates
131 TF number by determining the number of TFCs available to assemble into TFs (Sarikaya and
132 Extavour 2015). We reasoned that the genetic mechanisms of Hpo regulation of TF number might

133 be revealed by determining the responses of germ cells and somatic cells to Hpo signaling activity
134 during TF formation (Sarikaya and Extavour 2015). We therefore selected larvae over three
135 stages of early ovary morphogenesis as follows: (1) before TF formation (Early = 72 hAEL; Figure
136 1Bi); (2) during TF formation (Middle (mid) = 96 hAEL; Figure 1Bii); and (3) after TF formation
137 (Late = 120 hAEL; Figure 1 Biii). We expressed GFP specifically in either the somatic cells (red
138 cells in Figure 1C) or in the germ cells (blue cells in Figure 1C) using cell type-specific GAL4
139 drivers (Brand and Perrimon 1993) (see Methods) and isolated somatic and germ cells
140 respectively using Fluorescence-Activated Cell Sorting (FACS) (Supplemental Figure S1). We
141 had previously established the gene expression profiles of wild type somatic and germ cells at
142 these stages (Tarikere et al. 2021). In the present study, we used the UAS/GAL4 system (Brand
143 and Perrimon 1993) to knock down either *hpo* or *yki* in either somatic or germ cells across the
144 three developmental stages described above, and then performed tissue-specific RNA-Seq to
145 identify the transcriptional regulatory effects of these two main components of the Hpo signaling
146 pathway on larval ovary development and morphogenesis (Figure 1D-E).

147

148 **The Hpo pathway regulates gene expression differently in the ovarian germ line and soma**
149 Our RNA-Seq study produced 48 independent datasets (Supplemental Table S1) of gene
150 expression in germ cells and somatic cells in two different knockdown conditions and at three
151 developmental stages. To identify and understand the variation in gene expression across
152 samples, we performed a principal component analysis (PCA). Our results showed that 51.5% of
153 the variation across all datasets was explained by cell type (Figure 2A). The first principal
154 component clearly separated somatic cells from germ cells (PC1 in Figure 2A). Cell type-specific
155 gene expression included both genes with known roles in the germ line (e.g. *vasa* (Lasko and
156 Ashburner 1988) and *bruno* (Kim-Ha et al. 1995) or in the somatic gonad (e.g. *traffic jam* (Li et al.
157 2003) and *bab2* (Godt and Laski 1995), as well as novel genes without such roles previously

158 described (Supplemental Table S2). The second greatest impact on transcriptional variation
159 (PC2) was developmental stage (Figure 2A).

160 We then performed individual PCA analysis of somatic cells (Figure 2B) and germ cells
161 (Figure 2C), which allowed us to better observe the effects of the two RNAi knockdown conditions
162 on the sample clustering. In the somatic cells, most of the variation (32.3%) amongst the samples
163 was attributable to developmental stage rather than to genotype (stages are indicated as distinct
164 shapes along PC1 in Figure 2B). Along the PC2 axis, datasets were sorted by genotype, with
165 both the *hpo* and *yki* loss-of-function treatments segregating in opposite directions relative to the
166 control across all three developmental stages (colors along PC2 in Figure 2B). By contrast, in the
167 germ cells, the samples clustered by genotype rather than by stage (colors along PC1 in Figure
168 2C). The *hpo* and *yki* loss-of-function conditions clustered together independently of
169 developmental stage, but far from the respective controls (Figure 2C).

170 These results suggest that *yki* and *hpo* regulate transcriptional activity in ovarian germ
171 cells and somatic cells differently during larval development. In the soma, the two genes have
172 distinct and stage-specific impacts on the transcriptomic landscape. In contrast, loss of function
173 of both genes generates very similar effects on the transcriptomes of the germ line, and these
174 regulatory impacts do not change significantly across the period of development studied here. To
175 better understand this variation at the level of individual genes in each cell type sample, we
176 performed a differential gene expression (DGE) analysis of *hpo* and *yki* knockdown conditions
177 compared to the corresponding control samples at each stage. In general, we found more
178 differentially expressed genes in germ cells than in somatic cells, when either *hpo* or *yki* levels
179 were reduced (Figure 2D, Supplemental Table S3).

180 In the soma, there was a similar number of upregulated (365) and downregulated (310)
181 genes (17.7%) under *hpo* knockdown, compared to over 60% more upregulated (231) than
182 downregulated (143) genes (61.5%) under *yki* knockdown (Figure 2D, Supplemental Table S3).

183 In contrast, in the germ cells we observed on average over twice as many down-regulated genes
184 (1,161 and 1,120 under *hpo* and *yki* knockdown respectively) as upregulated genes (421 and 600
185 under *hpo* and *yki* RNAi respectively) in both knockdown conditions. Interestingly, this much larger
186 number of differentially expressed *hpo*- and *yki*-responsive genes in the germ line did not
187 correspond with a notable change of the germ line transcriptional landscape throughout the
188 developmental period under study (Figure 2C). The soma, on the other hand, exhibited distinct
189 gene expression responses to Hpo signaling over developmental time (Figure 2B), and these
190 differential responses were explained by a comparatively small number of genes (Figure 2D). We
191 had previously observed that in the somatic cells, the cell proliferation phenotypes induced by the
192 reduction of *hpo* and *yki* activity were diametrically opposed (Sarikaya and Extavour 2015).
193 Consistently, differential gene expression analysis of *hpo* and *yki* knockdown conditions showed
194 that in the soma, most of the differentially regulated genes (75%) were exclusive to each genotype
195 (*hpo RNAi* 55% and *yki* RNAi 20%) (Figure 2E). Of all the differentially expressed genes, the
196 expression of only four genes (*apterous*, *CG11400*, *wrapper*, and *expansion*) was significantly
197 affected in opposite ways by *hpo* and *yki* RNAi treatment (Figure 2E). By contrast, in the germ
198 cells the majority (51%) of the differentially expressed genes were common to both *hpo* and *yki*
199 loss of function conditions (869 commonly downregulated and 245 commonly upregulated), and
200 only one gene (*CG34408*) showed an “opposite” expression change (upregulated in *yki* loss of
201 function and downregulated in *hpo* loss of function) (Figure 2F). These results are consistent with
202 the above-described observations that *yki* and *hpo* knockdowns induced similar changes in the
203 germ line transcriptome (Figure 2C), but induced genotype-specific effects on the transcriptome
204 of the soma (Figure 2B).

205

206 **Functional prediction analysis of the differentially expressed genes**

207 The differentially expressed genes in the germ cells included more significantly enriched
208 pathways from the Kyoto Encyclopedia of Genes and Genomes (KEGG) and terms from the Gene
209 Ontology (GO) database than the genes differentially expressed in the soma (Figure 3,
210 Supplemental Figure S2). We found that the Hippo, MAPK, Hedgehog, and TGFβ pathways were
211 significantly enriched among the downregulated genes in the germ line under both *hpo* and *yki*
212 knockdown conditions (Figure 3). We additionally found that DNA replication and mismatch repair
213 pathways were enriched within the genes upregulated in response to *hpo* knockdown in germ
214 cells. In the germ line response to *yki* knockdown, we observed enriched GO terms relevant to
215 meiosis and cell cycle regulation (Supplemental Figure S2a). In contrast, somatic ovarian cells
216 displayed very few significantly altered pathways under either knockdown condition (Figure 3).
217 GO analysis revealed that members of some of the same processes that were downregulated in
218 the germ line, were downregulated in somatic *hpo* knockdowns, but with fewer gene counts than
219 those in germ cells (Supplemental Figure S2). These processes included cell adhesion, taxis,
220 motility, tissue growth, cell proliferation, stem cell population maintenance, maintenance of cell
221 number, cell proliferation and cell death.

222

223 ***yki* is downregulated under *hpo* knockdown in the germ line but not the soma**

224 Our previous work suggested that Yki functions downstream of Hpo in the soma but independently
225 of Hpo in the germ line (Sarikaya and Extavour 2015). We used our cell-type-specific
226 transcriptomes to determine whether this functional difference was reflected at the level of
227 transcript regulation in one or both of germ line and soma. As expected, we observed a significant
228 reduction (adjusted p-value<0.05) of *hpo* transcript levels across all stages and in both cell types
229 under *hpo* knockdown (Figure 4A). The levels of *yki* transcript were also down-regulated (adjusted
230 p-value<0.05) by *yki* RNAi in all stages and in both cell types, with two apparent exceptions

231 (Figure 4B). First, we noted that the 1.4-fold downregulation of *yki* under *yki* RNAi in early-stage
232 somatic cells just missed our significance threshold (adjusted p-value 0.055). Furthermore,
233 somatic cells at this stage displayed a different transcriptional landscape than controls, consistent
234 with *yki* knockdown (Figure 2B). Second, we noted that one of the control samples for mid stage
235 germ cells had anomalously low levels of *yki* transcript compared to other control samples of the
236 same and other stages (outlined in red in Figure 4B). Removal of this putative outlier revealed a
237 significant reduction of *yki* under yki RNAi (Supplemental Figure S3). Thus, we conclude that both
238 RNAi conditions were able to significantly reduce the transcript levels of their respective target
239 genes, and that our analytical methods were able to detect this reduction.

240 In terms of the effect of RNAi against these two genes on the transcript levels of the other,
241 we found that *yki* transcript levels were significantly reduced under *hpo* RNAi in late stage germ
242 cells, but not at earlier stages, and not in any stage in the soma (Figure 4B).*yki* RNAi (log2FC=-
243 1) and the *hpo* RNAi (log2FC=-0.8) conditions caused a similar reduction in *yki* transcript in the
244 germ line at this late stage. In contrast, the knockdown of *yki* did not yield a significant change in
245 *hpo* transcript levels in either cell type at any stage (Figure 4A). A possible exception may be the
246 mid stage germ cells: when the control sample with anomalously low levels of *yki* is excluded,
247 *hpo* appears significantly downregulated under *yki* knockdown with a fold change of -1.1
248 (Supplemental Figure S3). The degree of possible down-regulation of *hpo* in the *yki* RNAi
249 condition is much weaker (Log2FC=-1.1) than the reduction of *hpo* produced by the *hpo* RNAi
250 condition at the same stage (Log2FC=-4.1) (Figure 4A). Taken together, our results suggest that
251 the transcriptional regulatory relationship between *hpo* and *yki* in the larval female germ line is
252 complex, different from that in the soma, developmental stage-specific, and not directly predicted
253 from previous observations on the regulatory interactions of their protein products.

254

255 **Gene regulatory network analysis suggests *chinmo* as a novel mediator of *hpo*-dependent**
256 ***yki* regulation**

257 To generate hypotheses as to how *hpo* might regulate *yki* expression in the larval germ line, we
258 performed a network analysis. To this end, we built a directed network using the DroID database
259 of protein-protein interactions and transcription factor-encoding genes (Murali et al. 2011; Yu et
260 al. 2008). Additionally, we used publicly available Yki and GAF Chip-seq data from *D.*
261 *melanogaster* embryo, wing disc and S2 cells (Oh et al. 2013) to find possible direct targets of Yki
262 in *D. melanogaster* and added them into the network. From the ChIP-seq Yki data, we identified
263 1,513 peaks of Yki-binding regions, which we mapped to the closest gene, thus identifying 1,118
264 genes putatively regulated by Yki across the three studied cell types. By taking the intersection of
265 sets of putative Yki targets from all three cell types, we hoped to retrieve targets of Yki that might
266 also be relevant in the ovary.

267 In the germ line, 31.4% and 33.4% respectively of all the genes downregulated in either
268 *hpo* or *yki* knockdowns were putative direct targets of Yki (Supplemental Figure S4). Conversely,
269 of the 1,118 putative Yki targets in our network that were differentially expressed, most of them
270 were downregulated (94.59% under *hpo* RNAi and 79.14% under *yki* RNAi) (Supplemental Figure
271 S4). In contrast, in somatic cells only 8.23% and 2.86% of putative Yki target genes were
272 significantly affected by *hpo* and *yki* knockdowns respectively (Supplemental Figure S4).
273 Similarly, among the differentially expressed putative Yki targets the downregulated fraction was
274 much lower in the somatic cells than observed in the germ cells (67.37% were downregulated
275 under *hpo* knockdown, and 50% under *yki* knockdown; Supplemental Figure S4). This is
276 consistent with the overall much higher number of differentially regulated *hpo*- and *yki*-responsive
277 genes in the germ cells relative to somatic cells (Figure 2D)

278 We found that the shortest path linking *hpo* and *yki* in the network was through a predicted
279 interaction of Hpo with a transcription factor called Chronologically inappropriate morphogenesis

280 (Chinmo), which was predicted to regulate *yki* expression (Figure 4C). Moreover, Chinmo was the
281 sole candidate in our interaction network that was predicted to directly link both Hpo and Yki
282 (Figure 4C). Our RNA-Seq data showed that this transcription factor is significantly upregulated
283 in late stage germ cells under both *hpo* and *yki* loss of function conditions, and conversely, was
284 significantly downregulated in late stage somatic cells under both RNAi conditions (Supplemental
285 Figure S5). We therefore considered the hypothesis that differential *chinmo* expression and/or
286 function between germ line and soma might contribute to the different responses of those cell
287 types to Hpo pathway activity and sought to test this hypothesis experimentally.

288

289 **Nuclear Chinmo in the Germ cells is regulated by *yki* expression**

290 Our RNA-Seq results indicated that *chinmo* is expressed at constant levels in wild type germ line
291 cells throughout the developmental stages studied here, while levels of *chinmo* decreased over
292 developmental time in the ovarian somatic cells (Supplemental Figure S5). Given that *chinmo*
293 encodes a transcription factor (Zhu et al. 2006; Chen et al. 2020), we used an anti-Chinmo
294 antibody to examine the expression of Chinmo protein in the cells of the larval ovary. We detected
295 high levels of Chinmo protein in the nuclei of the germ cells in mid and late stages of larval
296 development, but only weak expression in the somatic ovarian cells (Figure 5A).

297 To determine the functional significance of *chinmo* expression in the larval ovary, we
298 reduced *chinmo* expression in either the somatic cells or the germ line cells. We used ovariole
299 number as a measure of effective change in phenotype in comparison with the *RNAi* knockdowns
300 of our predicted interactors of Chinmo in this context, Hpo and Yki, both of which we previously
301 identified as regulating ovariole number (Sarikaya and Extavour 2015). We found that, consistent
302 with the weakly detected Chinmo protein in the soma, reduction of *chinmo* in the somatic cells,
303 unlike the reduction of either *hpo* or *yki,* caused no significant change in ovariole number (Figure
304 5B; Supplemental Table S4). In contrast, abrogation of *chinmo* in the germ cells caused a

305 significant increase in ovariole number, as did reduction of *hpo* in the germ cells (Figure 5B;
306 Supplemental Table S4). Reducing levels of y*ki* in the germ cells did not cause any change in
307 ovariole number (Figure 5B; Supplemental Table S4).

308 Our network model predicted a putative transcriptional regulatory relationship between *yki*
309 and *chinmo*, and a potential protein-protein interaction between Hpo and Chinmo proteins. We
310 therefore asked whether levels of *yki* or *hpo* gene activity influenced the levels of Chinmo protein
311 in the developing ovary. Consistent with our network model, Chinmo protein levels were not
312 significantly affected by *hpo RNAi* (Figure 5C). Similarly, reduction of *chinmo* or *yki* expression in
313 somatic cells did not significantly alter detectable Chinmo protein levels in germ cells (Figure 5C;
314 Supplemental Table S4). However, Chinmo protein levels did significantly increase in the germ
315 cells upon *hpo* knockdown in somatic cells (Figure 5C; Supplemental Table S4), indicating a non-
316 cell autonomous role for Hpo in Chinmo regulation in the germ line. Reduction of *chinmo* or *yki* in
317 the germ line caused a reduction in detectable Chinmo protein in these cells (Figure 5C;
318 Supplemental Table S4).

319 To understand the functional outcomes in the ovary of Chinmo levels in the larval germ
320 cells (Figure 5C; Supplemental Table S4), we quantified germ cells, TFCs, and TFs at the late
321 larval stage, and ovarioles in the adult, under loss of germ line expression of *chinmo*, *yki* and *hpo*.
322 Reduction of *chinmo*, but not *yki* or *hpo*, in the germ cells led to a significant increase in germ cell
323 number when compared to both *GAL4* or *[RNAi]* controls (Figure 5D; Supplemental Table
324 S4). We found that the increase in ovariole number caused by reduction of *chinmo* or *hpo* in the
325 germ cells (Figure 5B; Supplemental Table S4) was the result of a non-cell-autonomous increase
326 in TFC number and in TF number (Figure 5E; Supplemental Table S4). Interestingly, reduction in
327 *chinmo* levels in the germ line also caused an increase in the number of TFCs in each TF (Figure
328 5E; Supplemental Table S4). Consistent with the observation that *yki* reduction in germ cells did

329 not change ovariole number (Figure 5B; Supplemental Table S4), this genetic background also
330 had wild type numbers of TFCs and TFs (Figure 5E; Supplemental Table S4).

331 Taken together, these data are consistent with the hypothesis that Chinmo protein in the
332 nucleus of germ cells regulates germ cell number cell-autonomously, and that Chinmo protein
333 levels in the germ line require germ line expression of *yki*. Further, expression of *chinmo* and
334 *hippo* in the germ cells also exerts a non-cell autonomous effect on somatic cells, limiting TFC
335 number, TF number, and hence ovariole number.

336

337 **DISCUSSION**

338 We have provided evidence for a novel genetic mechanistic hypothesis to explain the differential
339 response of germ line and somatic cells to the Hpo signaling pathway during the larval
340 development of the *D. melanogaster* ovary. We propose that the transcription factor Chinmo acts
341 as a modifier of Hpo-independent cell number regulation of the germ line, but not of the somatic
342 gonad cells.

343

344 **The Hippo pathway has distinct effects on transcription in the germ cells and the soma of**
345 **the larval ovary**

346 In this study, we knocked down either *hpo* or *yki* using RNAi driven in either the germ cells or the
347 somatic cells, thus providing us with a lens into the effects of each of these genetic manipulations
348 on the transcriptomic landscapes in each cell type. The canonical understanding of the Hippo
349 signaling pathway suggests that the presence of phosphorylated Hpo in the cellular milieu
350 prevents the nuclear localization of Yki and therefore the downstream expression of its target
351 genes. Under this model, the absence of Hpo in the cytoplasm allows Yki to remain

352 unphosphorylated, enter the nucleus, and drive the expression of its downstream targets. This
353 model therefore predicts a different transcriptional profile with and without Hpo. Our observation
354 that knockdown of either *hpo* or *yki* in the soma impacted transcript levels of two mutually
355 exclusive sets of genes supports the canonical understanding of the Hippo signaling pathway
356 (Figure 2B). In the germ cells, however, this is not the case: the effects of the knockdown of either
357 *hpo* or *yki* caused transcriptional changes in a similar set of genes (Figure 2C). This suggests that
358 *hpo* and *yki* RNAi have different effects on the transcriptome of the soma, but similar effects on
359 germ line.

360 Furthermore, we found that more genes were differentially expressed in the germ line than
361 in the soma (Figure 2D). The higher number of differentially expressed *yki*-regulated genes in
362 somatic tissues could mean that *yki* directly or indirectly represses more genes in somatic tissue
363 than it activates. Again, we observed differences in the effect of *hpo* and *yki* knockdown on germ
364 cells and somatic cells. The higher number of downregulated genes in the germ cells under these
365 conditions suggests that *hpo* and *yki* may operate in germ line tissue primarily through promoting
366 the transcription of genes rather than repressing them. In all genetic backgrounds, we observed
367 that most of the transcriptional variation in the soma was attributable to the progression of
368 development (Figure 2B), while in the germ line, the greatest variation between the samples was
369 due to abrogation of Hippo signaling pathway function (Figure 2C). This suggests that many of
370 the transcriptome differences we observed in the soma across development reflect the dynamic
371 morphogenetic changes taking place in the somatic cells of the ovary during the process of
372 terminal filament determination and organization.

373

374 ***Hpo* RNAi in germ cells does not affect cell number via *yki* repression**

375 The similar transcriptomic impact of *yki* and *hpo* knockdowns in the germ cells is intriguing given
376 their opposite phenotypic effects on cell proliferation in the soma (Sarikaya and Extavour 2015).
377 We had previously shown that *hpo* knockdown in somatic cells increased their number, while *yki*
378 knockdown decreased their number (Sarikaya and Extavour 2015). Similarly, overexpression of
379 *hpo* and *yki* in somatic cells and in germ cells also had opposite phenotypic effects, whereby *hpo*
380 overexpression reduced somatic cell number and *yki* knockdown increased it (Sarikaya and
381 Extavour 2015). These results were consistent with the canonical model of Hippo pathway activity.
382 However, although *yki* knockdown in germ cells decreased germ cell number, *hpo* knockdown did
383 not change it. We suggest that transcriptional regulation of *yki* by *hpo* may contribute to the
384 previously reported apparent imperviousness of germ cell number to *hpo* knockdown. We noted
385 that in the germ line, a reduction in *hpo* caused a reduction in *yki* (Figure 4B), but that there was
386 no detectable regulation of *hpo* by *yki* (Figure 4A). To our knowledge, this is the first reported
387 example of the transcriptional regulation of *yki* by *hpo.* We hypothesize that when *hpo* is reduced
388 in germ cells, although nuclear localization of Yki is not inhibited, there is less *yki* transcript. This
389 could in principle lead to less Yki protein and less efficient triggering of the transcriptional cascade
390 that would result in a cell number increase. In sum, we hypothesize that a balance of *hpo* and *yki*
391 transcript levels contributes to regulating the number of germ cells.

392

393 ***Chinmo* and its role in the regulation of *hpo* and *yki***

394 The transcription factor *chinmo* is the only gene we found in our network analysis predicted to
395 directly regulate *yki* in response to *hpo* levels, since Hpo and Chinmo proteins have the potential
396 to interact based on yeast two hybrid data (Yu et al. 2008). Furthermore, our network predicts that
397 *chinmo* has the potential to regulate the expression of both *hpo* and *yki*, and that in turn, *yki* could
398 regulate the expression of Chinmo based on ChIP-seq data (Oh et al. 2013). We hypothesize that
399 *chinmo* could be involved in regulating *yki* transcript levels in response to Hpo activity levels,

400 which would provide a mode of control of Hpo by Yki through Chinmo. Previous studies of *chinmo*
401 in the *D. melanogaster* testis and ovaries showed that it plays a key role in inducing male fate in
402 somatic cells of the testis, but that it is not required in ovarian somatic cells (Ma et al. 2016).
403 Consistent with that report, our results show increased expression of *chinmo* in response to *yki*
404 knockdown in the germ line but not in the soma (Supplemental Figure S5).

405 Chinmo is a BTB-Zinc finger transcription factor that is conserved across insects (Spokony
406 and Restifo 2007; Nadimpalli et al. 2015). Chinmo was first identified as a negative regulator of
407 the JAK/STAT signalling pathway (Flaherty et al. 2009; Fisher et al. 2012; Wang et al. 2013) and
408 acts as a transcriptional repressor downregulating the expression of a broad spectrum of genes
409 including *shotgun* (*E-Cadherin*) (Enomoto et al. 2021), *β Spectrin*, *polychaetoid*, *scribble* and
410 *mirror* (Grmai et al. 2021). In some studied contexts, Chinmo prevents the differentiation of cells
411 and promotes their ability to proliferate (Chafino et al. 2023) .

412 Given the low levels of detectable Chinmo in somatic nuclei of the larval ovary (Figure
413 5A), and that adult ovariole number is unchanged by somatic reduction of *chinmo* (Figure 5C), we
414 hypothesize that Chinmo does not act in somatic cells to impact the known regulation of the
415 number of TFCs, TFs or ovarioles by *hpo* or *yki* (Sarikaya and Extavour 2015). In contrast, we
416 detected Chinmo protein in larval germ cell nuclei (Figure 5A), where its expression appears to
417 be dependent on *yki* levels in the germ cells (Figure 5C). Further, we observed that reduction of
418 *chinmo* in germ cells caused an increase in germ cell number (Figure 5D), suggesting that Chinmo
419 acts in larval ovarian germ cells to limit their proliferation. This is reminiscent of the observation
420 that in $chinmo^{ST}$ loss of function mutants, adult male germ cells overproliferate (Ma 2014) . On
421 the other hand, $chinmo^{-/-}$ clones in a heterozygous $chinmo^{+/-}$ background do not (Tseng 2021) .
422 Thus, the cell-autonomous impact of *chinmo* function on germ cell proliferation appears to be
423 context- and sex-specific. Combining the results presented herein with our previous

424 understanding of Hippo signaling in the ovary, we propose a model for the cell type-specific
425 regulation of *hpo*-mediated proliferation during larval ovary development (Figure 6).

426 In this model, Chinmo and Yki function in opposition to each other in the germ line to
427 regulate germ cell number, limiting or promoting germ cell proliferation respectively. Thus, unlike
428 in the somatic cells, loss of *hpo* in germ cells does not cause an increase in germ cell number
429 because Chinmo continues to prevent Yki-dependent transcription. The similarities that we
430 observed between the transcriptional profiles of the *hpo* and *yki* knockdown in the germ cells
431 might be explained by the prediction that Chinmo prevents Yki-dependent transcription in these
432 cells. Thus, we propose that the interplay of Chinmo and Yki levels in the nucleus contributes to
433 the maintenance of germ cell number, and that disrupting this balance causes a change in germ
434 cell number. This model is also consistent with the Hpo-independent function of Yki in the germ
435 cells that was suggested by our previous work (Sarikaya and Extavour 2015).

436

437 **Cell-non-autonomous effects of Chinmo and Hippo**

438 Reduction of somatic *hpo* causes a non-autonomous increase in the levels of detectable nuclear
439 Chinmo in the germ cells (Figure 5C). This could be due to *hpo* downregulation in either or both
440 of TFCs or intermingled cells, given that the GAL4 driver we used here (*tj:Gal4*) is expressed in
441 both somatic cell types (Sarikaya and Extavour 2015). We note that downregulation of *hpo* in
442 intermingled cells causes JAK/STAT pathway upregulation in germ cells (Sarikaya and Extavour
443 2015), and that Chinmo is positively regulated by the JAK/STAT signalling pathway (Flaherty et
444 al. 2009; Fisher et al. 2012; Wang et al. 2013). It is thus possible that abrogating *hpo* activity in
445 intermingled cells causes nuclear Chinmo levels to rise in the germ line because of the non-
446 autonomous upregulation of JAK/STAT activity in germ cells.

447 Our observation of the non-autonomous impact of germ cell number on multiple aspects
448 of TFC number and organization (Figure 5B, 5E) is a new and intriguing finding. Reducing *chinmo*
449 or *hpo* in the germ line led to a significant increase in TFC, TF (Figure 5E) and ovariole number
450 (Figure 5B), suggesting that germ cell number can positively regulate ovariole number, a
451 hypothesis that has remained underexplored in the field. In our previous work (Sarikaya and
452 Extavour 2015) we did not observe a statistically significant increase in germ cells in
453 *nos:GAL4>hpo*^{RNAi} larval ovaries (Sarikaya and Extavour 2015), which is the same genetic
454 background we used in the present work. Further, although we did not count ovarioles in our
455 previous analysis of the *nos:GAL4>hpo*^{RNAi} condition, we did not observe a statistically significant
456 non-autonomous impact of *hpo* knockdown in the germ line on terminal filament cell number. We
457 attribute these differences to the fact that the control genotypes used for comparison and
458 calculation of statistical significance in the present work (GAL4 or UAS heterozygotes obtained
459 by crossing the parent strains to wild type strain Oregon R), were slightly different from the control
460 genotypes used in our previous study (sibling controls) (Sarikaya 2015) . We and others have
461 observed that ovariole number, and its contributing developmental processes, are such highly
462 polygenic traits that even small changes in genetic background can have statistically detectable
463 effects (Coyne 1991,Thomas-Orillard 1976,Bergland 2008,Orgogozo 2006,Telonis-Scott
464 2005,WAYNE 2001,Wayne 2002,Kumar 2020) .

465 Although increasing ovariole number by increasing germ cell number has not, to our
466 knowledge, previously been reported, there are at least two reported examples of the inverse
467 situation, where reduced ovariole number is correlated with reduced germ cell number. In one
468 example, ovaries of adult females carrying the dominant female sterile *ovo*^{D1} allele, which lacks
469 functional adult female germ cells, have fewer ovarioles than wild type (Extavour 2000). This could
470 in principle be because of a reduction in total germ cell number during larval stages in this
471 genotype, which is consistent with the interpretation of larval germ line clonal analysis of this allele

472 (Perrimon 1984). In a second example, agametic adult females generated by irradiating the
473 posterior pole of embryos (Geigy 1931), have fewer ovarioles than controls (Aboïm 1945).

474 Finally, we note that reduction in *chinmo* levels in the germ cells also caused an
475 unexpected increase in the number of TFCs in each TF (Figure 5E). To our knowledge, this is the
476 first reported evidence of changes in germ line gene influencing TCF number and TF
477 morphogenesis. Determining the non-autonomous regulatory mechanism that allows larval germ
478 cells to impact the future fecundity of the adult, by influencing somatic morphogenesis of the
479 ovary, is an interesting avenue for future research.

480

481 **MATERIALS AND METHODS**

482

483 **Fly stocks**

484 Flies were reared as previously described (Sarikaya et al. 2012) at 25ºC and 60% humidity on
485 standard *Drosophila* food with yeast in uncrowded vials. The "wild type" genetic background
486 referred to herein is Oregon R (Lindsley and Grell 1968). The following fly lines were obtained
487 from the Bloomington *Drosophila* Stock Center (BDSC): *w[*]; P{w[+mW.hs]=GawB}bab1[Pgal4-*
488 *2]/TM6B, Tb[1]* (abbreviated herein as *bab:GAL4*; BDSC stock number 6803); *P{w[+mC]=UAS-*
489 *Dcr-2.D}1, w[1118]; P{w[+mC]=GAL4-nos.NGT}40* (abbreviated herein as *nos:GAL4*; BDSC
490 stock number 25751); *y w; P{w[+mW.hs]=GawB}NP1624* was obtained from the Kyoto Stock
491 Centre (abbreviated herein as *tj:*GAL4; stock number K104–055); *y[1] v [1];*
492 *P(y[+t7.7]v[+t1.8]=TRiP. HMS00006) attP2* (abbreviated herein as *hpo[RNAi]*; BDSC stock
493 number 33614) and *y[1] v[1]; P(y[+t7.7] v[+t1.8]=TRiP.HMS00041)attP2* (abbreviated herein as
494 *yki[RNAi]*; BDSC stock number 34067); *y[1] v[1]; P{y[+t7.7] v[+t1.8]=TRiP.JF02341}attP2*
495 (abbreviated herein as *chinmo[RNAi]*; BDSC stock number 26777). *w[1118], P[UAS Stinger]*

496 (abbreviated herein as *UAS:Green Stinger I*, (Barolo et al. 2000) used for GFP expression was
497 a gift from Dr. James Posakony (University of California, San Diego). Crosses (described below
498 in "Staging larvae") were set with 100-200 virgin females and 50-100 males in a 180 ml bottle
499 (with 50 ml media per bottle) one day prior to egg laying. For somatic *chinmo* knockdown via
500 RNAi, we used a *tj:GAL4* driver (Li et al. 2003), rather than the *bab*:*GAL4* driver (Cabrera et al.
501 2002), as the latter caused lethality when driving *chinmo [RNAi]* (data not shown).

502

503 **Staging larvae**

504 Uniformly staged larvae were collected from near-synchronously laid eggs. To obtain a desired
505 genotype, crosses were set as described above in "Fly Stocks" at 25°C at 60% humidity and left
506 overnight to mate. Hourly egg collections were set up on 60 mm apple juice-agar plates (9 g agar,
507 10 g sugar, 100 ml apple juice and 300 ml water) with a pea-sized spread of fresh yeast paste
508 (baker's yeast granules made into a paste with a drop of tap water). Eggs were collected hourly
509 for eight hours. The first two collection plates were discarded to remove asynchronously laid eggs
510 that may have been retained inside the females following fertilization. Staged first instar larvae
511 were collected into vials 24 hours after egg collection. Larvae at 72h hours After Egg Laying (h
512 AEL) were designated as early stage, at 96h AEL as middle stage and at 120h AEL as late stage
513 of terminal filament development.

514

515 **Dissection and dissociation of larval ovaries**

516 Staged larvae were collected for dissection every hour. Fat bodies were dissected out of the
517 larvae using a pair of forceps. Ovaries, located in the center of the length of each fat body, were
518 then dissected free of the fat body using an insulin syringe needle (BD 328418). Ovaries thus
519 dissected clear of fat body were collected in ice-cold DPBS (Thermo Fisher 14190144) and

520 batches of 20-30 ovaries in DPBS were kept on ice for a maximum of four hours until dissociation
521 and subsequent FACS processing. For dissociation, dissected ovaries in ice-cold DPBS were
522 transferred to 0.25% trypsin solution (Thermo Fisher 25200056) for ten minutes at room
523 temperature in the cavity of a glass spot plate (Fisher Scientific 13-748B). They were then
524 transferred to another cavity containing 2.5% liberase (5 g liberase reconstituted in 2 ml nuclease
525 free water; Sigma 5401119001), teased apart with tungsten needles until most of the clumps were
526 separated, and left in the liberase solution (without agitation) at room temperature for ten minutes.
527 The tissue in liberase was pipetted gently to uniformly mix and dissociate the cells. The cell
528 suspension was then transferred to an RNA Lobind tube (Eppendorf 8077-230) and placed on a
529 vortexer for 1 minute. This sample was immediately subjected to fluorescence activated cell
530 sorting (FACS) and the sorted cell suspension was collected in an RNA Lobind tube containing
531 100-200 µl Trizol (Thermo Fisher 15596026).

532

533 **Flow sorting GFP positive cells**

534 The dissociated cell suspension was sorted in a MoFlo Astrios EQ Cell sorter (Beckman Coulter)
535 run with Summit v6.3.1 software. The dissociated cell suspension was diluted and a flow rate of
536 200 events per second was maintained with < 98% sorting efficiency during the sorting process.
537 A scatter gate (R1) was employed to eliminate debris, and a doublet gate (R2) was used to
538 exclude non-singlet cells. A 488 nm emission Laser was used to excite the GFP, and the collection
539 was at 576 nm. The GFP-positive cells were designated in gate R3 and sorted directly into Trizol
540 (Supplemental Table S1). The resulting cells collected in Trizol were frozen immediately by
541 plunging the tube in liquid nitrogen and then stored at -80°C until RNA extraction. A single
542 replicate consisted of at least 1000 cell counts pooled from FACS runs.

543

544 **RNA extraction**

545 Flow sorted cells stored in Trizol at -80°C were thawed at room temperature and lysed with a
546 motorized pellet pestle (Kimble 749540-0000). A Zymo RNA Micro-Prep kit (Zymo Research
547 R2060) was used to isolate RNA from the homogenized Trizol preparations. An equal volume of
548 molecular grade ethanol (Sigma E7023) was added to Trizol and mixed well with a pellet pestle,
549 then pipetted onto a spin column. All centrifugation steps were done at 10,000g for one minute at
550 room temperature. The column was washed with 400 µl Zymo RNA wash buffer and then treated
551 with Zymo DNase (6 U/µl) for 15 minutes at room temperature. The column was then washed
552 twice with 400 µl Zymo RNA Pre-wash buffer and once with Zymo RNA wash-buffer. The RNA
553 was eluted from the column in 55 µl of nuclease-free water (Thermo Fisher 10977015). The RNA
554 obtained was quantified first using a NanoDrop (Model ND1000) spectrophotometer and then
555 using a high sensitivity kit (Thermo Fisher Q32852) on a Qubit 3.0 Fluorometer (Thermo Fisher
556 Q33216). The RNA was also checked for integrity on a high sensitivity tape (Agilent 5067-5579)
557 with an electronic ladder on an Agilent Tapestation 2200 or 4200.

558

559 **Library preparation**

560 cDNA libraries were prepared using the Takara Apollo library preparation kit (catalogue #
561 640096). Extracted RNA samples were checked for quality using Tapestation tapes. 50µl of RNA
562 samples were pipetted into Axygen PCR 8-strip tubes (Fisher Scientific 14-222-252) and
563 processed through PrepX protocols on the Apollo liquid handling system. mRNA was isolated
564 using PrepX PolyA-8 protocol (Takara 640098). The mRNA samples were then processed for
565 cDNA preparation using the PrepX mRNA-8 (Takara 640096) protocol. cDNA products were then
566 amplified for 15 cycles of PCR using longAmp Taq (NEB M0287S). During amplification PrepX
567 RNA-Seq index barcode primers were added to each library to enable multiplexing. The amplified
568 library was then cleaned up using PrepX PCR cleanup-8 protocol with magnetic beads (Aline C-

569 1003). The final cDNA libraries were quantified using a high sensitivity dsDNA kit (Thermo Fisher
570 Q32854) on a Qubit 3.0 Fluorometer (Thermo Fisher Q33216). cDNA content and quality were
571 assessed with D1000 (Agilent 5067-5582) or high sensitivity D1000 tape (Agilent 5067-5584, for
572 low quantities of cDNA) on an Agilent Tapestation 2200 or 4200.

573

574 **Sequencing cDNA libraries**

575 Libraries were sequenced on an Illumina HiSeq 2500 sequencer. Single-end 50bp reads were
576 sequenced on a high-throughput flow cell. Libraries of varying concentrations were normalized to
577 be equimolar, the concentrations of which ranged between 2-10nM per lane. All the samples in a
578 flow cell were multiplexed and later separated based on unique prepX indices to yield at least 10
579 million reads per library. The reads were demultiplexed and trimmed of adapters using the
580 bcl2fastq2 v2.2 pipeline to yield final fastq data files.

581 Three RNA-Seq biological replicates were obtained for each condition, each of which had
582 at least 10 million reads. The only exception was the early-stage germ line under both *hpo* and
583 *yki* RNAi knockdowns, for which we only obtained a single biological replicate due to the technical
584 challenge of obtaining enough germ line cells from these knockdown ovaries. These single
585 replicates of early germ line stages were not included in the differential expression analysis but
586 are made publicly available as part of the reported dataset (See Data Availability).

587

588 **Immunohistochemistry**

589 Larvae were dissected as previously described (Sarikaya et al. 2012; Sarikaya and Extavour
590 2015) and stained as previously described. For all cell counts, samples were dissected at the
591 larval-pupal transition stage. Primary antibodies and the concentrations used to stain the larval-
592 pupal transition stage ovaries are as follows: Mouse anti- Engrailed 4D9 (1:40, Developmental

593 Studies Hybridoma Bank (DSHB)), Rabbit anti-Vasa (1:3000, gift from A. Nakamura, Kumamoto
594 University), Rat anti-Chinmo (1:500, gift from E. Bach, New York University; (Wu 2012).
595 Secondary antibodies used were anti-mouse Alexa Fluor 488, anti-rat Alexa Fluor 488, and anti-
596 rabbit Alexa Fluor 568, all used at 1:400, and Hoechst 33342 used at 1:10,000 (stock solution 10
597 mg/mL). All samples were imaged on a Zeiss LSM 880 inverted laser confocal microscope. For
598 quantification of Chinmo expression levels, all samples were dissected and stained in parallel.
599 Imaging settings, including laser power, detector gain and step sizes, were kept constant for all
600 experimental and appropriate control samples.

601

602 **Quantification of ovariole number, cell number and Chinmo protein level**

603 Ovariole number was quantified as previously described (Kumar et al. 2020) . Germ cells were
604 counted manually in larval-pupal transition stage ovaries stained for Vasa protein, using the
605 Manual tracking with TrackMate plugin in Fiji (Schindelin et al. 2012; Tinevez et al. 2017) .
606 Terminal filaments and terminal filament cells in each terminal filament were counted manually in
607 larval-pupal transition stage ovaries stained for Engrailed, using the Cell counter plugin in Fiji.
608 Total terminal filament cell number per ovary was calculated by adding up the number of terminal
609 filament cells in each terminal filament.

610

611 **RNA-Seq data processing**

612 The *D. melanogaster* genome assembly and gene annotations were obtained from FlyBase
613 version dmel_r6.36_FB2020_05 (Larkin et al. 2020) . The reads were aligned with RSEM v1.3.3.
614 (Li and Dewey 2011) Using STAR v2.7.6a as read aligner, (Dobin et al. 2013) we obtained the
615 gene counts in each library. Because some of the tissue-specific biological samples were
616 sequenced in more than one lane or run, the reads were split into multiple fastq files, and the

617 gene counts belonging to the same biological sample were summed. Gene counts in each dataset
618 were normalized with the variance stabilizing transformation (VST) method implemented in the
619 DESeq2 v1.26.0 (Love et al. 2014) R package. Further analyses, such as principal component
620 analysis, hierarchical clustering, and differential expression analysis, were performed in R using
621 the VST-normalized counts.

622

623 **Differential expression analysis**

624 The differential expression analyses were performed with DESeq2 v1.26.0 (Love et al. 2014).
625 Genes with a Benjamini-Hochberg adjusted p-value lower than 0.05 were selected as differentially
626 expressed in the corresponding contrast.

627

628 **Functional predictions**

629 The Gene Ontology (GO) and Kyoto Encyclopedia of Genes and Genomes (KEGG) pathways
630 enrichment analyses were performed on the differentially expressed genes with the enrichGO
631 and enrichKEGG functions of the clusterProfiler package (v3.14.3) for R (Yu et al. 2012). The GO
632 terms were obtained using the R package AnnotationDbi (Carlson 2024) with the database
633 org.Dm.eg.db v3.10.0. The GO overrepresentation analysis of biological process was performed
634 against the gene universe of all *D. melanogaster* annotated genes in org.Dm.eg.db, adjusting the
635 p-values with the Benjamini-Hochberg method, adjusted p-value and q-value cutoff of 0.01, and
636 a minimum of 30 genes per term. For the KEGG enrichment analysis, p-values were adjusted by
637 the Benjamini-Hochberg procedure, and an adjusted p-value cutoff of 0.05 was used.

638

639 **Analysis of publicly available ChIP-Seq data**

640 We obtained the ChIP-Seq from GEO (GSE46305 and GSE38594) (Oh et al. 2013, 2014). We
641 downloaded the coordinates of the 3,749, 6,491, and 3,991 Yorkie-bound peaks from embryo
642 (E8-16h), wing imaginal discs, and S2 cells respectively. The coordinates of the peaks were
643 based on the *D. melanogaster* genome assembly BDGP release 5, and transformed to
644 coordinates for the latest genome version (release 6) with the lifterOver function. The peaks were
645 annotated with ChIPseeker (v.1.22.1) using *D. melanogaster* genome annotations from FlyBase
646 (v6.36). We defined the promoter region as the 1,500 bp flanking the transcription start site, and
647 69-75% of the peaks were found within the promoter regions of genes thus defined. In total 2,331,
648 3,931, and 2,247, genes with Yki-bound sites in the defined promoter region were identified, in
649 embryo, wing imaginal discs, and S2 cells respectively. 4,980 genes were unique (appeared only
650 in one dataset), 1,118 were common across the three datasets, and 2,406 were common to at
651 least two datasets. Following the same methodology, we analyzed the GAF (*Trl*) Chip-Seq peaks
652 (GSE38594) from embryo (E8-16h) and wing imaginal discs. Thus, we associated the 6,449 and
653 6,302 GAF-bound peaks from embryo and wing imaginal discs respectively to the promoters of
654 4,086 genes, of which 2,095 were common to both datasets.

655

656 **Network analysis**

657 We obtained the Transcription Factor – Gene (TF-gene) interaction network form the Drosophila
658 Interactions database (www.droidb.org, version DroId_v2018_08), containing 157,462
659 interactions of 12,323 genes. We added to this network the 1,118 interactions of Yorkie and the
660 2,095 interactions of GAF predicted from the ChIP-seq analysis. After removing redundancies,
661 we had 158,923 edges and 112,562 nodes in the network. We also obtained 127,353 unique
662 protein-protein interactions (PPI) between 10,632 proteins from DroID v2018_08. The TF-gene
663 and PPI networks were joined, yielding a network with 328,989 edges and 13,337 nodes while

designating as an edge attribute whether the interaction was a TF-gene or PPI. We assigned directionality to the TF-gene edges because TFs regulate the target and not vice-versa while the PPI edges were set as bi-directional. We looked for the shortest path in the network in which Hpo could regulate Yki, and Chinmo emerged as the only possible connector, requiring only two steps.

COMPETING INTERESTS STATEMENT

The authors declare no competing interests.

ACKNOWLEDGEMENTS

We thank the flow cytometry and genomics staff at the Bauer Core Facility of Harvard University Faculty of Arts and Sciences for advice on FACS sorting and sequencing, and members of the Extavour lab for helpful discussions. This work was supported by NIH R01 award R01-HD073499-0 to CGE, by funds from Harvard University, and by the Google Cloud Academic Research Credits Program. CGE is a Howard Hughes Medical Institute investigator.

AUTHOR CONTRIBUTIONS

ST performed all steps in generating individual transcriptome datasets, including experimental design, ovary dissection and dissociation, RNA-Seq library preparation and sequencing. GY performed all statistical and network analyses of transcriptome data. TK performed and analysed genetic experiments testing the role of *chinmo*. CGE conceived of the project, provided oversight and funding. All authors drafted and edited the manuscript.

686 **DATA AVAILABILITY**

687 All the raw data are publicly available at NCBI-Gene Expression Omnibus (GEO) database under
688 the accession code GSE250320. Control datasets for early, mid and late-stage germ line and
689 somatic cells are accessible as a part of the NCBI-GEO database under the accession code
690 GSE172015 (GSM5239772-89). The scripts used to process and analyze the data are available
691 at the GitHub repository https://github.com/guillemylla/Ovariole_morphogenesis_RNAseq,
692 commit ID 171064d.

693 **REFERENCES**

694

695 Barolo S, Carver LA, Posakony JW. 2000. GFP and -Galactosidase Transformation Vectors for
696 Promoter/Enhancer Analysis in Drosophila. *BioTechniques* **29**: 726–732.

697 Barresi MJF, Gilbert SF. 2023. Developmental Biology.

698 Besse F, Busson D, Pret A. 2005. Hedgehog signaling controls Soma-Germen interactions
699 during Drosophila ovarian morphogenesis. *Dev Dynam* **234**: 422–431.

700 Brand AH, Perrimon N. 1993. Targeted gene expression as a means of altering cell fates and
701 generating dominant phenotypes. *Development* **118**: 401–415.

702 Büning J. 1994. Chapter 3. In *The Insect Ovary, Ultrastructure, previtellogenic growth and*
703 *evolution*, pp. 31–324.

704 Carlson M. 2024. AnnotationDbi: Introduction To Bioconductor Annotation Packages.
705 https://bioconductor.org/packages/release/bioc/html/AnnotationDbi.html.

706 Chen H-M, Marques JG, Sugino K, Wei D, Miyares RL, Lee T. 2020. CAMIO: a transgenic
707 CRISPR pipeline to create diverse targeted genome deletions in Drosophila. *Nucleic Acids*
708 *Res* **48**: 4344–4356.

709 Church SH, Medeiros BAS de, Donoughe S, Reyes NLM, Extavour CG. 2021. Repeated loss of
710 variation in insect ovary morphology highlights the role of development in life-history
711 evolution. *Proc Royal Soc B* **288**: 20210150.

712 David J. 1970. Le nombre d'ovarioles chez Drosophila melanogaster: relation avec la fécondité
713 et valeur adaptative. *Achives de Zoologie experimentale et generale* **111**: 357–370.

714 Dobin A, Davis CA, Schlesinger F, Drenkow J, Zaleski C, Jha S, Batut P, Chaisson M, Gingeras
715 TR. 2013. STAR: ultrafast universal RNA-seq aligner. *Bioinformatics* **29**: 15–21.

716 Dong J, Feldmann G, Huang J, Wu S, Zhang N, Comerford SA, Gayyed MF, Anders RA, Maitra
717 A, Pan D. 2007. Elucidation of a Universal Size-Control Mechanism in Drosophila and
718 Mammals. *Cell* **130**: 1120–1133.

719 Enomoto M, Takemoto D, Igaki T. 2021. Interaction between Ras and Src clones causes
720 interdependent tumor malignancy via Notch signaling in Drosophila. *Dev Cell* **56**: 2223-
721 2236.e5.

722 Extavour CGM. 2007. Gray anatomy: phylogenetic patterns of somatic gonad structures and
723 reproductive strategies across the Bilateria. *Integr Comp Biol* **47**: 420–426.

724 Fisher KH, Wright VM, Taylor A, Zeidler MP, Brown S. 2012. Advances in genome-wide RNAi
725 cellular screens: a case study using the Drosophila JAK/STAT pathway. *BMC Genom* **13**:
726 506.

727 Flaherty MS, Zavadil J, Ekas LA, Bach EA. 2009. Genome-wide expression profiling in the
728 Drosophila eye reveals unexpected repression of notch signaling by the JAK/STAT pathway.
729 *Dev Dyn* **238**: 2235–2253.

730 Godt D, Laski FA. 1995. Mechanisms of cell rearrangement and cell recruitment in Drosophila
731 ovary morphogenesis and the requirement of bric a brac. *Development* **121**: 173–187.

732 Grmai L, Harsh S, Lu S, Korman A, Deb IB, Bach EA. 2021. Transcriptomic analysis of
733 feminizing somatic stem cells in the Drosophila testis reveal putative downstream effectors of
734 the transcription factor Chinmo. *G3 Genes Genomes Genetics* **11**: jkab067-.

735 Hodin J. 2009. Chapter 11. She Shapes Events As They Come: Plasticity in Female Insect
736 Reproduction. In *Phenotypic Plasticity of Insects* (ed. D.W. Whitman).

737 Honěk A. 1993. Intraspecific Variation in Body Size and Fecundity in Insects: A General
738 Relationship. *Oikos* **66**: 483.

739 Huang J, Wu S, Barrera J, Matthews K, Pan D. 2005. The Hippo Signaling Pathway
740 Coordinately Regulates Cell Proliferation and Apoptosis by Inactivating Yorkie, the
741 Drosophila Homolog of YAP. *Cell* **122**: 421–434.

742 Kim-Ha J, Kerr K, Macdonald PM. 1995. Translational regulation of oskar mRNA by Bruno, an
743 ovarian RNA-binding protein, is essential. *Cell* **81**: 403–412.

744 King R. 1970. *Ovarian Development in Drosophila Melanogaster*. Academic Press.

745 King RC, Aggarwal SK, Aggarwal U. 1968. The development of the female Drosophila
746 reproductive system. *J Morphol* **124**: 143–165.

747 Kumar T, Blondel L, Extavour CG. 2020. Topology-driven protein-protein interaction network
748 analysis detects genetic sub-networks regulating reproductive capacity. *Elife* **9**: e54082.

749 Larkin A, Marygold SJ, Antonazzo G, Attrill H, dos Santos G, Garapati PV, Goodman JL,
750 Gramates LS, Millburn G, Strelets VB, et al. 2020. FlyBase: updates to the Drosophila
751 melanogaster knowledge base. *Nucleic Acids Res* **49**: D899–D907.

752 Lasko PF, Ashburner M. 1988. The product of the Drosophila gene vasa is very similar to
753 eukaryotic initiation factor-4A. *Nature* **335**: 611–617.

754 Li B, Dewey CN. 2011. RSEM: accurate transcript quantification from RNA-Seq data with or
755 without a reference genome. *BMC Bioinform* **12**: 323.

756 Li MA, Alls JD, Avancini RM, Koo K, Godt D. 2003. The large Maf factor Traffic Jam controls
757 gonad morphogenesis in Drosophila. *Nat Cell Biol* **5**: 994–1000.

758 Lindsley DL, Grell EH. 1968. *Genetic Variations of Drosophila melanogaster*. Carnegie
759 Institution of Washington, Washington, DC, USA.

760 Love MI, Huber W, Anders S. 2014. Moderated estimation of fold change and dispersion for
761 RNA-seq data with DESeq2. *Genome Biol* **15**: 550.

762 Ma Q, Cuevas M de, Matunis EL. 2016. Chinmo is sufficient to induce male fate in somatic cells
763 of the adult Drosophila ovary. *Development* **143**: 754–763.

764 Manning SA, Kroeger B, Deng Q, Brooks E, Fonseka Y, Hinde E, Harvey KF. 2024. The
765 Drosophila Hippo pathway transcription factor Scalloped and its co-factors alter each other's
766 chromatin binding dynamics and transcription in vivo. *Dev Cell* **59**: 1640-1654.e5.

767 Markow TA, O'Grady PM. 2007. Drosophila Biology in the Genomic Age. *Genetics* **177**: 1269–
768 1276.

769 Matsuoka S, Hiromi Y, Asaoka M. 2013. Egfr signaling controls the size of the stem cell
770 precursor pool in the Drosophila ovary. *Mech Dev* **130**: 241–253.

771 Moon S, Kim W, Kim S, Kim Y, Song Y, Bilousov O, Kim J, Lee T, Cha B, Kim M, et al. 2017.
772 Phosphorylation by NLK inhibits YAP-14-3-3-interactions and induces its nuclear localization.
773 *EMBO Rep* **18**: 61–71.

774 Murali T, Pacifico S, Yu J, Guest S, Roberts GG, Finley RL. 2011. DroID 2011: a
775 comprehensive, integrated resource for protein, transcription factor, RNA and gene
776 interactions for Drosophila. *Nucleic Acids Res* **39**: D736–D743.

777 Nadimpalli S, Persikov AV, Singh M. 2015. Pervasive Variation of Transcription Factor
778 Orthologs Contributes to Regulatory Network Evolution. *PLoS Genet* **11**: e1005011.

779 Oh H, Irvine KD. 2008. In vivo regulation of Yorkie phosphorylation and localization.
780 *Development* **135**: 1081–1088.

781 Oh H, Slattery M, Ma L, Crofts A, White KP, Mann RS, Irvine KD. 2013. Genome-wide
782 Association of Yorkie with Chromatin and Chromatin-Remodeling Complexes. *Cell Rep* **3**:
783 309–318.

784 Oh H, Slattery M, Ma L, White KP, Mann RS, Irvine KD. 2014. Yorkie Promotes Transcription by
785 Recruiting a Histone Methyltransferase Complex. *Cell Rep* **8**: 449–459.

786 Rust K, Byrnes LE, Yu KS, Park JS, Sneddon JB, Tward AD, Nystul TG. 2020. A single-cell
787 atlas and lineage analysis of the adult Drosophila ovary. *Nat Commun* **11**: 5628.

788 Sarikaya DP, Belay AA, Ahuja A, Dorta A, Green DA, Extavour CG. 2012. The roles of cell size
789 and cell number in determining ovariole number in Drosophila. *Dev Biol* **363**: 279–289.

790 Sarikaya DP, Extavour CG. 2015. The Hippo Pathway Regulates Homeostatic Growth of Stem
791 Cell Niche Precursors in the Drosophila Ovary. *Plos Genet* **11**: e1004962.

792 Schindelin J, Arganda-Carreras I, Frise E, Kaynig V, Longair M, Pietzsch T, Preibisch S,
793 Rueden C, Saalfeld S, Schmid B, et al. 2012. Fiji: an open-source platform for biological-
794 image analysis. *Nat Methods* **9**: 676–82.

795 Slattery M, Voutev R, Ma L, Nègre N, White KP, Mann RS. 2013. Divergent Transcriptional
796 Regulatory Logic at the Intersection of Tissue Growth and Developmental Patterning. *PLoS*
797 *Genet* **9**: e1003753.

798 Song X, Call GB, Kirilly D, Xie T. 2007. Notch signaling controls germline stem cell niche
799 formation in the Drosophila ovary. *Development* **134**: 1071–1080.

800 Spokony RF, Restifo LL. 2007. Anciently duplicated Broad Complex exons have distinct
801 temporal functions during tissue morphogenesis. *Dev Genes Evol* **217**: 499–513.

802 Tapon N, Harvey KF, Bell DW, Wahrer DCR, Schiripo TA, Haber DA, Hariharan IK. 2002.
803 salvador Promotes Both Cell Cycle Exit and Apoptosis in Drosophila and Is Mutated in
804 Human Cancer Cell Lines. *Cell* **110**: 467–478.

805 Tarikere S, Ylla G, Extavour CG. 2021. Distinct gene expression dynamics in germ line and
806 somatic tissue during ovariole morphogenesis in Drosophila melanogaster. *G3 Genes*
807 *Genomes Genetics*.

808 Tinevez J-Y, Perry N, Schindelin J, Hoopes GM, Reynolds GD, Laplantine E, Bednarek SY,
809 Shorte SL, Eliceiri KW. 2017. TrackMate: An open and extensible platform for single-particle
810 tracking. *Methods* **115**: 80–90.

811 Wang H, Chen X, He T, Zhou Y, Luo H. 2013. Evidence for Tissue-Specific JAK/STAT Target
812 Genes in Drosophila Optic Lobe Development. *Genetics* **195**: 1291–1306.

813 Wang W, Xiao Z-D, Li X, Aziz KE, Gan B, Johnson RL, Chen J. 2015. AMPK modulates Hippo
814 pathway activity to regulate energy homeostasis. *Nat Cell Biol* **17**: 490–499.

815 Wu S, Huang J, Dong J, Pan D. 2003. hippo Encodes a Ste-20 Family Protein Kinase that
816 Restricts Cell Proliferation and Promotes Apoptosis in Conjunction with salvador and warts.
817 *Cell* **114**: 445–456.

818 Wu S, Liu Y, Zheng Y, Dong J, Pan D. 2008. The TEAD/TEF Family Protein Scalloped
819 Mediates Transcriptional Output of the Hippo Growth-Regulatory Pathway. *Dev Cell* **14**: 388–
820 398.

821 Xu T, Wang W, Zhang S, Stewart RA, Yu W. 1995. Identifying tumor suppressors in genetic
822 mosaics: the Drosophila lats gene encodes a putative protein kinase. *Development* **121**:
823 1053–1063.

824 Yatsenko AS, Shcherbata HR. 2021. Distant activation of Notch signaling induces stem cell
825 niche assembly. *Plos Genet* **17**: e1009489.

826 Yu G, Wang L-G, Han Y, He Q-Y. 2012. clusterProfiler: an R Package for Comparing Biological
827 Themes Among Gene Clusters. *OMICS: A J Integr Biol* **16**: 284–287.

828 Yu J, Pacifico S, Liu G, Finley RL. 2008. DroID: the Drosophila Interactions Database, a
829 comprehensive resource for annotated gene and protein interactions. *BMC Genom* **9**: 461.

830 Zhang L, Ren F, Zhang Q, Chen Y, Wang B, Jiang J. 2008. The TEAD/TEF Family of
831 Transcription Factor Scalloped Mediates Hippo Signaling in Organ Size Control. *Dev Cell* **14**:
832 377–387.

833 Zhao B, Wei X, Li W, Udan RS, Yang Q, Kim J, Xie J, Ikenoue T, Yu J, Li L, et al. 2007.
834 Inactivation of YAP oncoprotein by the Hippo pathway is involved in cell contact inhibition
835 and tissue growth control. *Genes Dev* **21**: 2747–2761.

836 Zhao B, Ye X, Yu J, Li L, Li W, Li S, Yu J, Lin JD, Wang C-Y, Chinnaiyan AM, et al. 2008. TEAD
837 mediates YAP-dependent gene induction and growth control. *Gene Dev* **22**: 1962–1971.

838 Zheng Y, Pan D. 2019. The Hippo Signaling Pathway in Development and Disease. *Dev Cell*
839 **50**: 264–282.

840 Zhu S, Lin S, Kao C-F, Awasaki T, Chiang A-S, Lee T. 2006. Gradients of the Drosophila
841 Chinmo BTB-Zinc Finger Protein Govern Neuronal Temporal Identity. *Cell* **127**: 409–422.

842

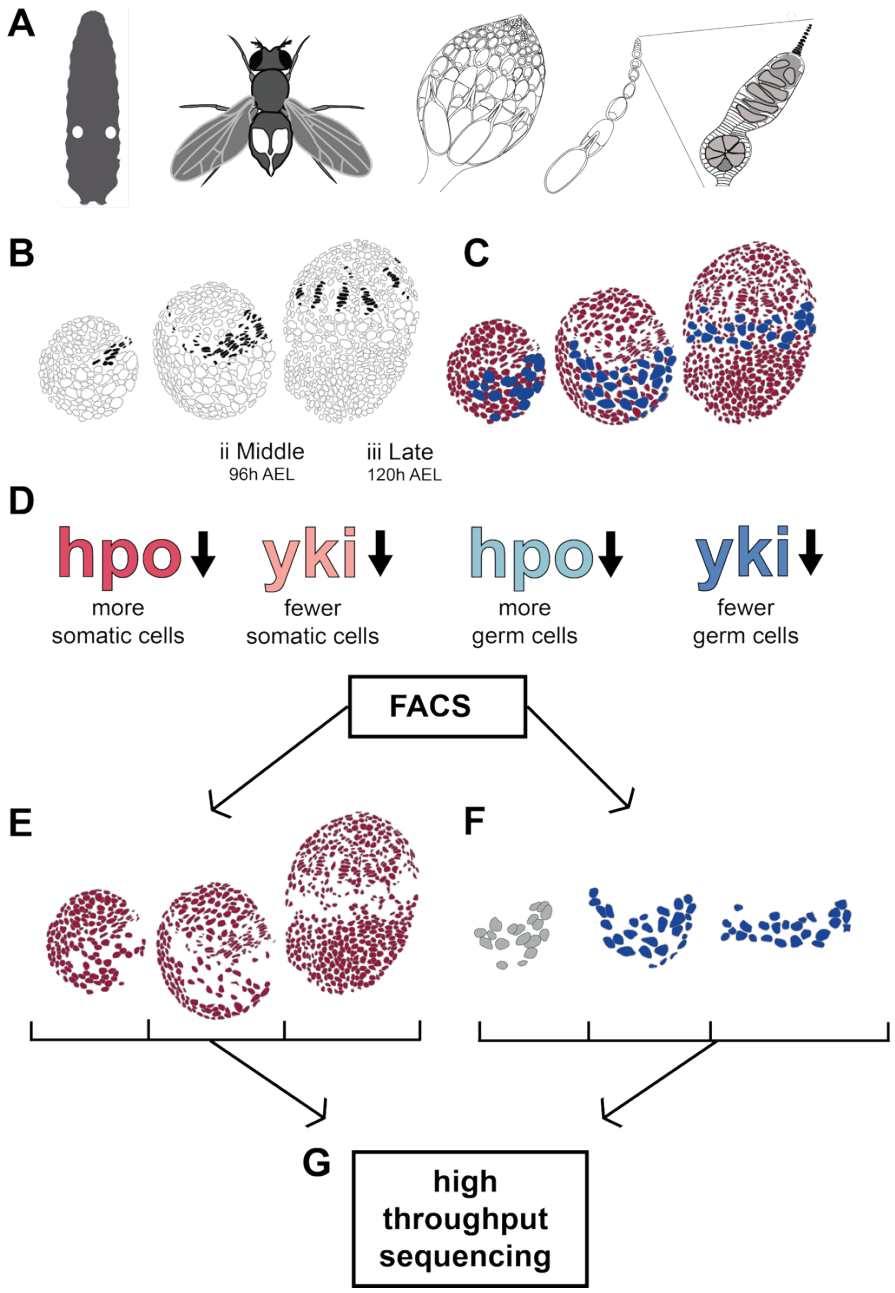

Figure 1: Experimental design to generate stage-specific transcriptomes of in somatic and germ line larval ovarian cells under wild type, *hpo* and *yki* loss of function conditions. (A) Left to right: Location of larval ovaries (indicated as white circles in the larva); location of adult ovaries in female abdomen (indicated in white within the abdomen); a single adult ovary; a single ovariole; a single germarium with terminal filaments in black. **(B)** The three developmental stages during terminal filament (in black) formation studied herein. **(C)** Somatic (red) and germ line (blue) cells were marked for FACS sorting using appropriate GAL4 drivers as described in Materials & Methods. **(D)** Summary of the tissue-specific RNAi knockdown treatments assessed at each stage in somatic and germ line cells. GFP labelled somatic cells **(E)** and germ cells **(F)** were sorted using FACS at the three developing stages of larval ovaries. Data from early-stage germ cells (grey), were not used for analysis; see Materials & Methods. **(G)** Sorted ovarian cell types were processed for mRNA extraction, cDNA library preparation and high throughput sequencing. h AEL = hours after egg laying.

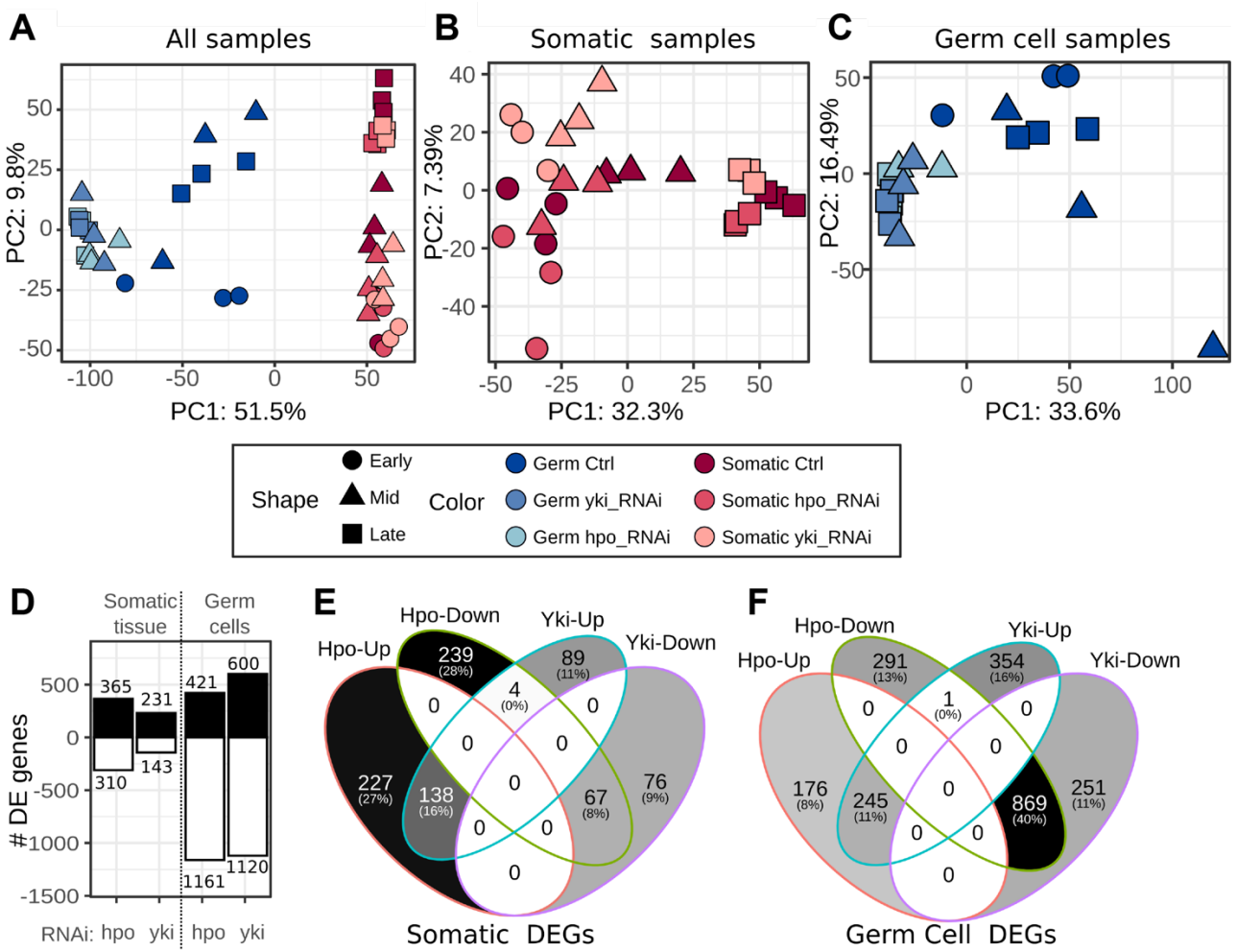

Figure 2: Distinct transcriptional impact of Hpo signaling on germ line and soma across ovarian development . (A) Principal Component Analysis (PCA) of all samples differentiates germ cells from somatic cells along PC1. (B) PCA of somatic transcriptomes showing clustering by time-point in PC1, and the knockdown effect in PC2. **(C)** PCA of germ line transcriptomes in which control and knockdown libraries cluster separately, but the *hpo* and *yki* knockdowns cluster together. **(D)** Number of significantly upregulated and downregulated genes (adjusted p-value < 0.05) in each cell type with grouped stages when comparing each knockdown to the control library. For somatic cells **(E)** and germ cells **(F)** a Venn diagram shows the differentially up- and down- regulated genes under each knockdown, including number and percentage of genes in each intersection.

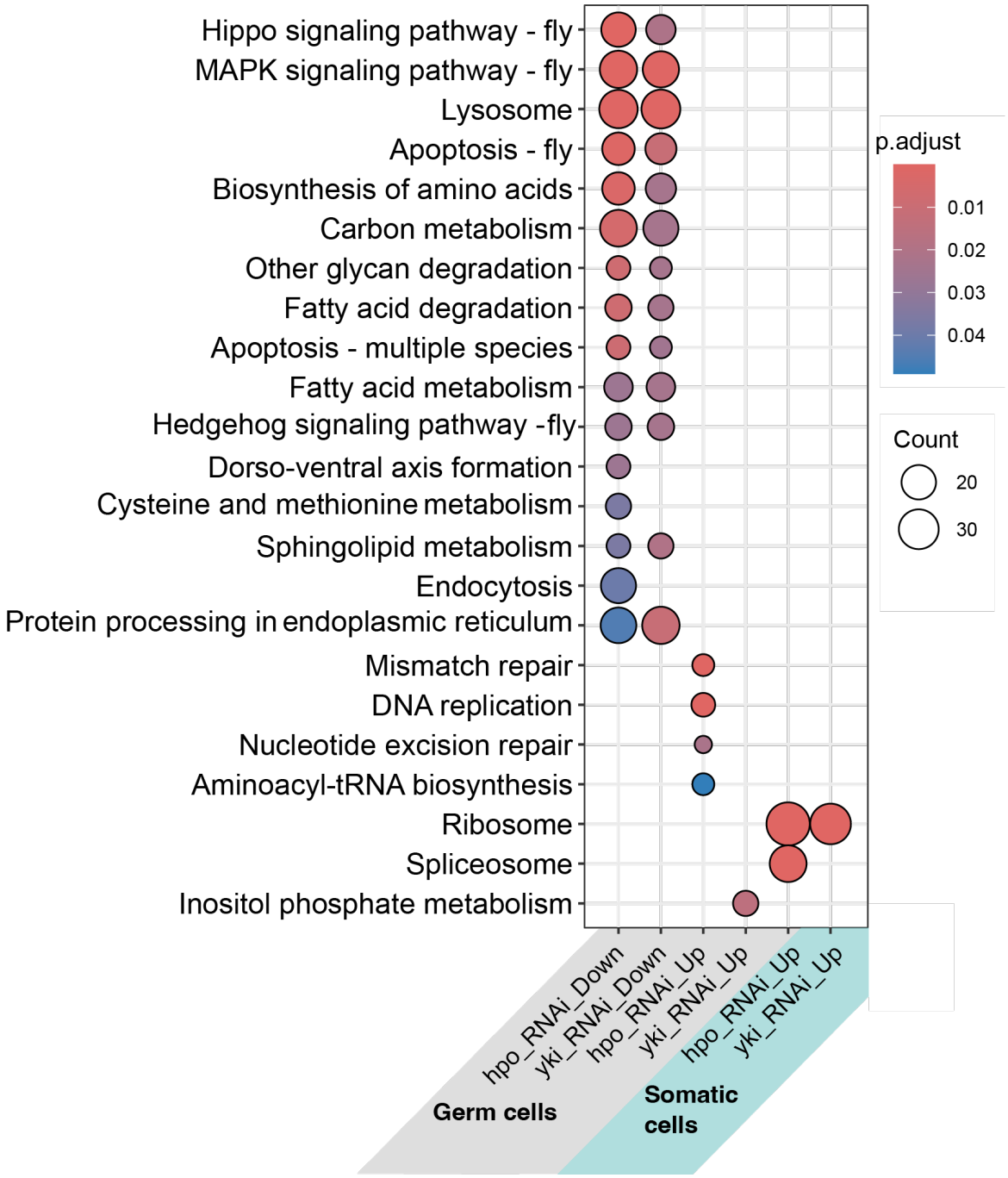

Figure 3: Perturbing *hpo* or *yki* levels has a larger transcriptomic impact on germ cells than somatic cells. Shown are significantly enriched (Benjamini-Hochberg adjusted p-value<0.05) KEGG pathways within the groups of significantly upregulated (Up) and downregulated (Down) genes in germ cells and somatic cells under *hpo* and *yki* RNAi conditions (grouping mid and late stages together).

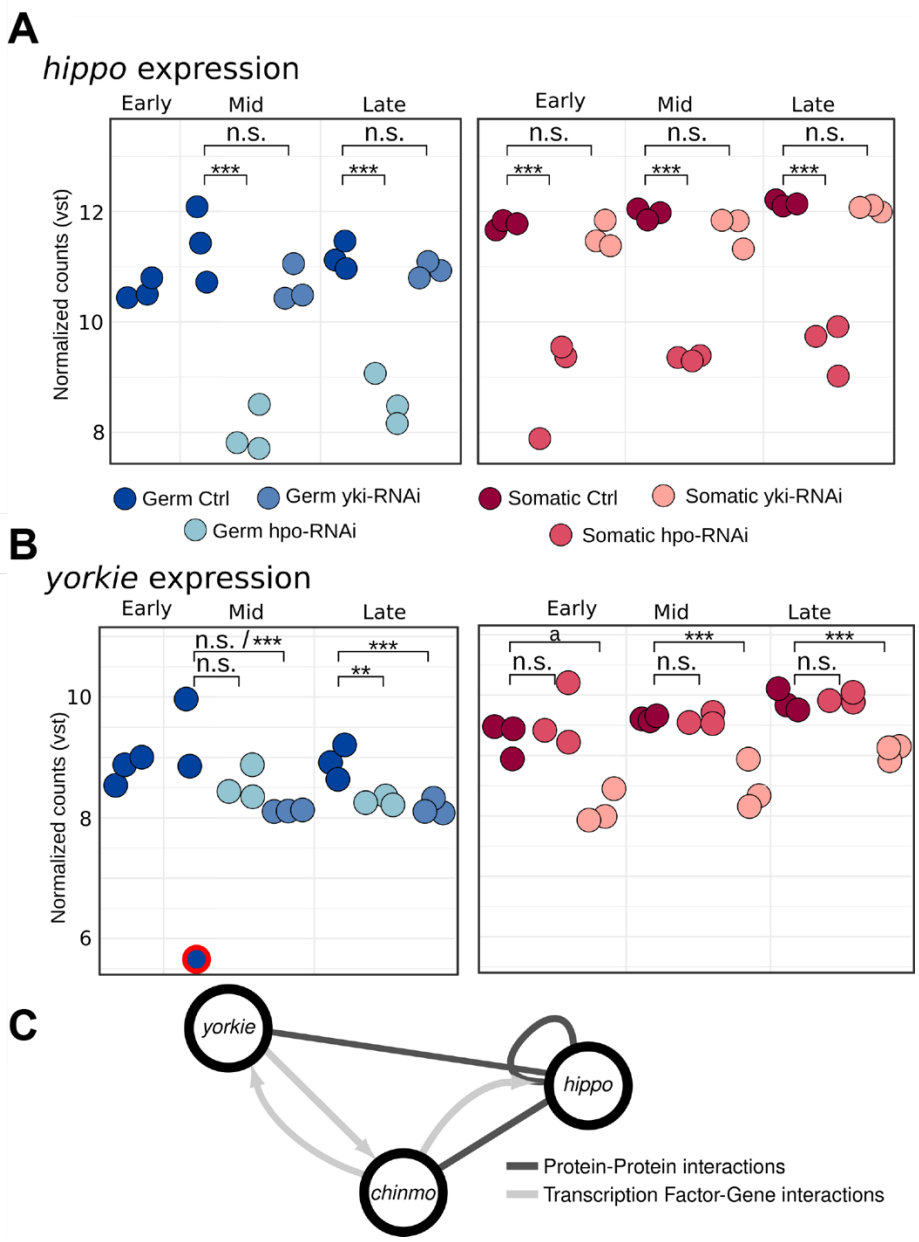

Figure 4: Prediction of chinmo as a novel germ cell-specific candidate regulator of *hpo* and/or *yki*. Expression of **(A)** *hpo* and **(B)** *yki* as vst-normalized counts in germ cells (left panels, blue dots) and somatic cells (right panels, red dots) in each RNA-Seq library (color shades indicate genetic condition). The *hpo* and *yki* transcripts appear significantly downregulated their corresponding RNAi conditions. The *yki* reduction in germ cells mid stages is significant when the control sample with anomalously low levels of *yki* (circled in red) is removed (Supplemental Figure S3). Additionally, *yki* appears significantly downregulated under *hpo* knockdown. Statistical significance levels from the differential expression analysis are codified as *** = adjusted p-value<0.01; ** = adjusted p-value<0.05; [a] = adjusted p-value = 0.055, n.s. = not significant. **(C)** Graph showing *hpo*, *yki*, and their only common direct neighbor in our network of protein-protein interactions, *chinmo*. Protein-protein candidate interaction edges are represented in dark grey, and transcription factor-gene candidate interactions are represented in light grey arrows with pointing to the gene predicted to be regulated by the TF. The TF *chinmo* appears has the potential to regulate both *hpo* and *yki*, can physically interact with *hpo*, and can potentially be regulated by *yki*.

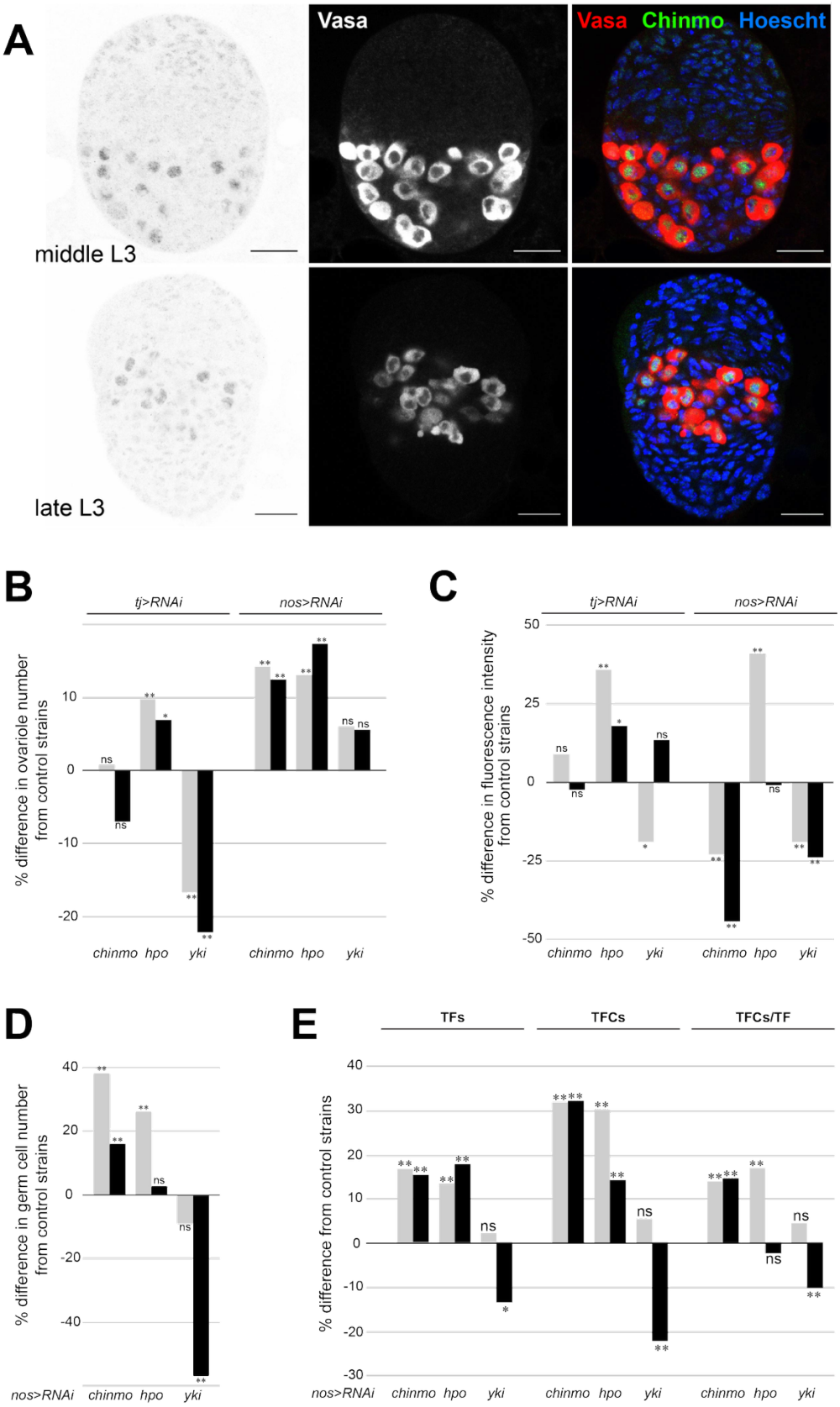
A
Vasa
Vasa Chinmo Hoescht
middle L3
late L3
B
tj>RNAi
nos>RNAi
% difference in ovariole number from control strains
chinmo hpo yki chinmo hpo yki
C
tj>RNAi
nos>RNAi
% difference in fluorescence intensity from control strains
chinmo hpo yki chinmo hpo yki
D
% difference in germ cell number from control strains
nos>RNAi chinmo hpo yki
E
TFs
TFCs
TFCs/TF
% difference from control strains
nos>RNAi chinmo hpo yki chinmo hpo yki chinmo hpo yki

884

885 **Figure 5: Chinmo regulates germ cell number autonomously and somatic cell number and**
886 **morphogenesis non-autonomously in the developing ovary. (A)** Chinmo is detected in germ cell
887 nuclei at mid and late stages of larval development. Red = Vasa; Chinmo = green, scale bars = 20μm.
888 **(B)** *chinmo RNAi* in the germ cells causes an increase in ovariole number. Percentage difference in
889 adult ovariole number where *UAS:chinmo [RNAi]*, *UAS:hippo [RNAi],* or *UAS:yorkie [RNAi]* are driven
890 in the somatic cells or in the germ cells. n=20 for each genotype. **(C)** Abrogation of Hpo signaling in
891 the germ cells causes a change in Chinmo levels in germ cell nuclei. Percentage difference in detected
892 fluorescence levels of Chinmo protein in larval ovarian germ cell nuclei where *UAS:chinmo [RNAi]*,
893 *UAS:hippo [RNAi]* or *UAS:yorkie [RNAi]* are driven in the somatic cells in the germ cells. $n \geq 50$ nuclei
894 from five ovaries. **(D)** *chinmo RNAi* in germ cells causes an increase in germ cell number. Percentage
895 difference in germ cell number where *UAS:chinmo [RNAi]*, *UAS:hippo [RNAi]* or *UAS:yorkie [RNAi]*
896 are driven in germ cells. **(E)** *chinmo* RNAi in germ cells causes an increase in Terminal Filament (TF)
897 number, Total Terminal Filament Cell (TFC) number and in the number of TFCs per TF. Percentage
898 differences in TF number and TFC number in each ovary, and the number of TFCs per TF where
899 *UAS:chinmo [RNAi]*, *UAS:hippo [RNAi]* or *UAS:yorkie [RNAi]* were driven in the germ cells. In **B**
900 through **E**, grey bars = comparisons to *Gal4* controls; blacks bars = comparisons to *UAS* controls.
901 Statistical significance was calculated using a student's two-tailed t-test with unequal variance. (** =
902 $p<0.01$, * = $p<0.05$, ns = $p>0.05$).

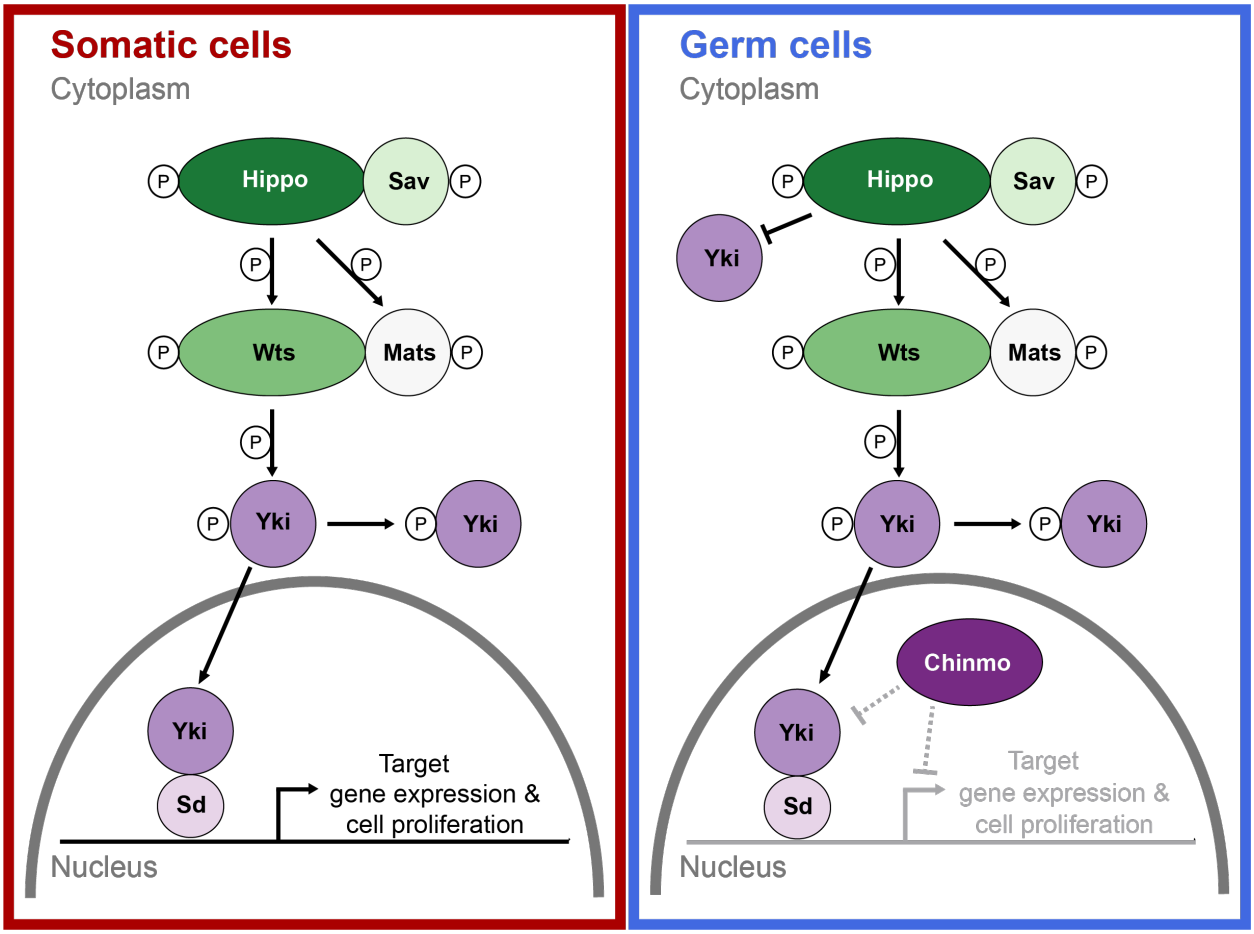

Figure 6. Hypothesis: Chinmo regulates Hpo signaling activity in the germ cells but not somatic cells. We previously showed that the components of the Hippo signaling pathway are present in both the germ and somatic cells, (Sarikaya 2015), and that the somatic cells (red) function under the influence of the canonical Hippo pathway (Sarikaya 2015). Under this model, the reduction of either *hpo* or *yki* causes a change in germ cell number. In germ cells (blue), Chinmo is present, which adds a secondary Hippo-independent repression of *yki*-dependent cell proliferation. Because our data cannot determine whether Chinmo acts directly on the localization of Yki to the nucleus, or indirectly by repressing cell proliferation downstream of Yki, the Chinmo-Yki relationship is indicated by grey dashed lines.